Journal of Inorganic and General Chemistry
ZAAC
Zeitschrift für anorganische und allgemeine Chemie
www.zaac.wiley-vch.de
RESEARCH ARTICLE
Check for updates
DOI: 10.1002/zaac.202500102
Konstanzer Online-Publikations-System (KOPS)
URL: http://nbn-resolving.de/urn:nbn:de:bsz:352-2-1cgkwdr1077443

Pnicturesque Luminescence: The Photophysical and Emissive Properties of Dipyridine Pyrrolide Group 15 Diiodide Complexes

Katharina L. Deuter, Björn Schneider, Kai Jellinek, and Rainer F. Winter*

We dedicate this work to Christian Limberg and Franc Meyer at the occasion of their 60th birthdays

The synthesis, characterization, and photophysical properties of a family of pnictogen complexes **Pn(DPP)I$_2$** bearing dipyridine pyrrolide (DPP$^-$) ligands and with As, Sb, and Bi as the central atom Pn are reported. Slight but systematic trends arising from the variation in the atomic number are apparent in NMR and UV–vis spectra. As confirmed by time-dependent density functional theory calculations, the electron-rich DPP$^-$ ligand endows the energetically lowest-lying electronic absorption band with partial DPP-to-Pn charge–transfer (ligand-to-metal charge transfer) character. All complexes are phosphorescent at cryogenic temperatures with high phosphorescence quantum yields of $\Phi_{phos} = 50.8$ to 83.9% and lifetimes in the range of tens of microseconds. In accordance with the heavy atom effect, merely **As(DPP)I$_2$**, the lightest representative of the three complexes within this work, displays weak fluorescence. It also possesses the shortest phosphorescence lifetime and the highest quantum yield for $^1O_2$ generation. This is attributed to a higher degree of covalent character of the Pn-ligand bonds and increased orbital overlap as well as larger iodide contributions to the LUMO.

1. Introduction

Recently, the heavier main group elements are receiving increasing attention for use as the central atom in devising photoluminescent materials.[1] The interest stems from several favorable attributes, such as high spin–orbit coupling (SOC) constants, and their higher natural abundance and better affordability compared to most transition metals, in particular the noble metals.[2] Exemplarily, a number of studies have shown that incorporation of iodine onto organic scaffolds may enhance intersystem crossing (ISC) and provide access to excited triplet states.[3] This propensity of heavy elements to accelerate ISC is known as the "heavy element effect" or "heavy atom effect" (HAE), which is rooted in the large SOC constants these elements inherently possess.[2] In addition, ISC may be enhanced if the respective heavy element is engaged in the molecular orbitals (MOs) that contribute to the corresponding electronic transition.[4] In coordination compounds of metal or metalloid main group elements, the central ions possess the ability to act as either electron donors in metal-to-ligand-charge transfer (MLCT) or as electron acceptors in ligand-to-metal charge transfer (LMCT) transitions. Thus, recent years have seen a number of publications focusing on the complexes of the group 13 and group 14 elements,[1a,1c,5] as well as the pnictogen elements As, Sb, and Bi.[6]

The elements across the pnictogen series display a wide variety of emissive properties. While photophysically active arsenic compounds commonly act as pure fluorescence or dual fluorescence and phosphorescence emitters,[7] complexes of antimony and bismuth have been reported to display fluorescence,[8] phosphorescence,[4c,9] or dually emissive behavior.[10] Despite the high potential of both Sb and Bi for generating excited triplet states through ISC, phosphorescence is often only observed at cryogenic temperatures, and the number of reports on pure phosphorescence emission at r.t. in solution remains rare.[4c,9a,9b,9d,11]

A number of literature reports compare the luminescent properties of Sb complexes with either their As or Bi congeners (refer to **Scheme 1**A for a selection).[7c,7d,12] Studies comparing the photophysical properties of homologous series of compounds of all three elements are more limited due to differing reactivity and solubility across the pnictogens.[6] In one such study, Inaba et al. reported on the emissive properties of the heavier pnictogen analogs of carbazole (cf. Scheme 1A),[13] which were shown to be emissive at cryogenic temperatures. While the phosphorous compound shows pure fluorescence, the arsole congener is dually emissive with fluorescence and phosphorescence, whereas the heavier stibole and bismole exhibit pure phosphorescence.[13] The impact of the heavy element effect was also studied at r.t. in CH_2Cl_2 for Pn(phenanthrenyl)$_3$ with Pn = P, Sb, and Bi (far right of Scheme 1A).[14] These complexes were fluorescent with violet ligand-centered emission. In these examples, the heavy element effect was most apparent in the decreasing quantum yield from the lighter to the heavier homologs.[14]

K. L. Deuter, B. Schneider, K. Jellinek, R. F. Winter
Faculty for Chemistry, University of Konstanz, Universitätsstrasse 10, 78457 Konstanz, Germany
E-mail: rainer.winter@uni-konstanz.de

Supporting information for this article is available on the WWW under https://doi.org/10.1002/zaac.202500102

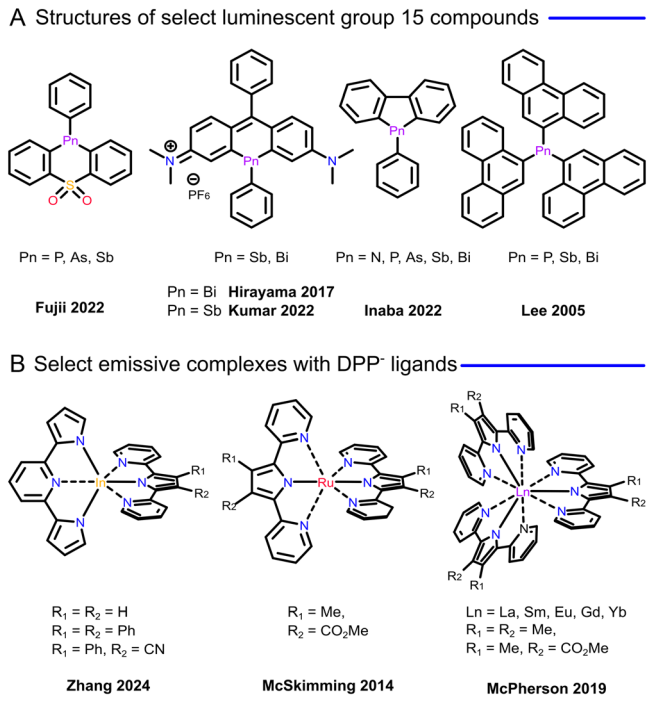

Scheme 1. A) Structures of select luminescent group 15 complexes. B) Select emissive complexes containing ligands with the DPP^{-} structural motif.

The propensity of bismuth to facilitate ISC in both *NCN* and *NNN* pincer complexes has been reported in recent years.[9c,9d,10b] It has previously been suggested that contributions of the bismuth atom to the molecular orbitals (MOs)volved in the lowest energy transition are beneficial for efficient ISC.[4c] Some of these studies focused on the emissive properties of Bi complexes with metal-centered ground states displaying MLCT character for their lowest energy transition.[4c,9d]

We recently reported on the emissive properties of bismuth complexes with LMCT-type character for their highest occupied molecular orbital (HOMO) to lowest unoccupied molecular orbital (LUMO) transitions. The ligand-centered ground state was achieved by the use of electron-rich dianionic pyridine dipyrrolide (PDP^{2-}) ligands, and these complexes exhibited phosphorescent emission in the red region of the spectrum.[9c] Recently, the PDP^{2-} ligand has been used in combination with indium in complexes of the In(PDP)(DPP) type (cf. Scheme 1B). These compounds are fluorescent at r.t. in solution and were used as photosensitizers for the photocatalytic reduction of carbon dioxide in concert with porphyrin complexes of Co, Ni, and Cu as the catalysts.[15] The DPP^{-} ligand displays similar properties to the PDP^{2-} ligand with regard to electron richness and rigidity and may also endow its complexes with high emission quantum yields. These favorable assets were already explored for the generation of fluorescent complexes of some lanthanides,[16] main group,[15] and transition metal elements (Scheme 1B).[17] Exemplarily, the emissive properties of complexes bearing ligands with the DPP^{-} structural motif have been explored in combination with Ru^{2+} (center of Scheme 1B), and these complexes exhibit weak fluorescence in the blue region of the spectrum.[17]

In this work, we aimed to combine the promising properties of the DPP^{-} ligand with the pnictogen metalloids arsenic, antimony, and bismuth and to investigate the influence of the HAE of these three elements on the photophysical and emissive properties of **Pn(DPP)I$_2$** complexes. The iodide ligands were employed to enhance the probability of ISC and to increase the stability of these complexes toward hydrolysis.

2. Results and Discussion

The synthesis of the ligand 2,2′-(1*H*-pyrrole-2,5-diyl)bis(pyridine) **HDPP** proceeded according to a modified literature procedure.[18] The synthesis starts from pyridine-2-carbaldehyde, which is subjected to a Stetter-type reaction with divinyl sulfone, catalyzed by 3-benzyl-5-(2-hydroxyethyl)-4-methylthiazol-3-ium chloride in order to obtain the diketone 1,4-di-2-pyridinyl-1,4-butanedione. The latter was then subjected to a Paal–Knorr pyrrole synthesis in neat ammonium acetate to give the proligand **HDPP** (see **Scheme 2**). Complexes **Pn(DPP)I$_2$** were then synthesized by deprotonation of **HDPP** with potassium hydride under inert conditions and subsequent reaction with the respective pnictogen iodide species PnI_3 to yield the complexes as bright orange (**As(DPP)I$_2$** and **Bi(DPP)I$_2$**) or yellow (**Sb(DPP)I$_2$**) powders in good to excellent yields (see Experimental Section for full details).

In mass spectra, the complexes appear as their cationic forms **Pn(DPP)I**$^{+}$, having lost one iodide ligand during the ionization process (cf. Figure S24, Supporting Information). Additionally, the complexes were characterized by ^{1}H- and ^{13}C- nucelar magnetic resonance (NMR) spectroscopy in either dimethyl sulfoxide

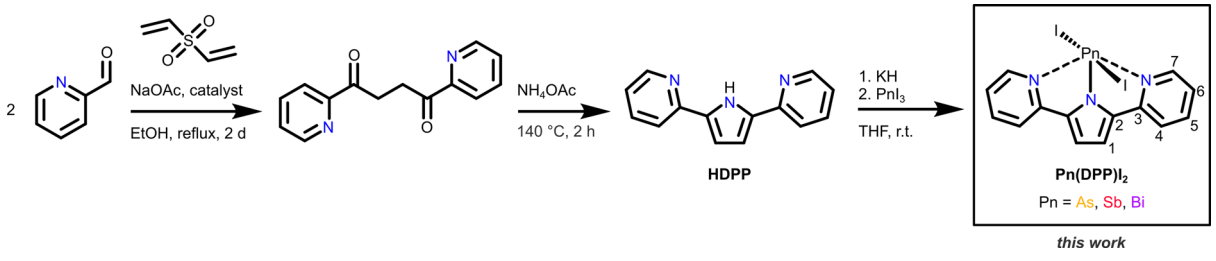

Scheme 2. Synthesis route pursued for the three complexes **Pn(DPP)I$_2$** described within this work. The catalyst in the first step is 3-benzyl-5-(2-hydroxyethyl)-4-methylthiazol-3-ium chloride.

(dmso)-d_6 or CD_2Cl_2 owing to differing solubilities and stabilities. While **Bi(DPP)I_2** and **Sb(DPP)I_2** are stable in dmso-d_6, even in the presence of residual water, **As(DPP)I_2** decomposes in less than 60 min (cf. Figure S23, Supporting Information) under the precipitation of a yellow solid. This process seems to be related to the water content in the solvent and occurs at a much slower rate in dmso-d_6 that was dried over molecular sieves. We thus succeeded in recording ^{1}H-NMR spectra of **As(DPP)I_2** in dry dmso-d_6 so that ^{1}H-chemical shifts can be compared (cf. **Table 1** and Figure S22, Supporting Information). The appreciably longer times needed to record ^{13}C- and 2D-NMR spectra of **As(DPP)I_2** nevertheless led to partial decomposition in this solvent, so that these data were recorded in dry CD_2Cl_2, in which the other two complexes were practically insoluble. Overall, we observe an increase in solubility from **Bi(DPP)I_2** to **As(DPP)I_2** while also observing a parallel decrease in tolerance toward moisture.

In accordance with the decreasing electronegativity along the pnictogen series, the ^{1}H-NMR resonance signals are shifted upfield from the heavier to the lighter congeners such that the ordering **As(DPP)I_2** > **Sb(DPP)I_2** > **Bi(DPP)I_2** applies to the shift of all ^{1}H-NMR signals with the exception of H-7 adjacent to the pyridinyl nitrogen atom (refer to Scheme 2 for atom numbering). The latter resonance remains rather invariant across this series. Compared to the proligand, the resonance signal of proton H-5 is affected the most by complexation, shifting from 7.78 ppm to up to 8.27 ppm for **As(DPP)I_2**. Table 1 summarizes all ^{1}H-NMR shifts of the complexes **Pn(DPP)I_2** in dmso-d_6.

We were able to grow single crystals suitable for single-crystal X-ray diffraction of **Bi(DPP)I_2** by slow evaporation of tetrahydrofuran (THF) from a saturated solution in this solvent. **Bi(DPP)I_2** crystallizes in the monoclinic space group *C*2/*c* with one molecule of **Bi(DPP)I_2** and 0.5 THF solvent molecules within the asymmetric unit. Two molecules of **Bi(DPP)I_2** associate as mutually iodide bridged dimers with *d*(Bi1-I1) = 3.1148(5) Å, *d*(Bi1-I2) = 2.9965(5) Å, and *d*(Bi1…I2′) = 3.5221(4) Å. The geometry around the central bismuth ion can be described as distorted pentagonal bipyramidal with the three nitrogen atoms of the ligand, the iodine atom of a neighboring molecule and the oxygen atom of the THF solvent molecule spanning the pentagonal base of the pyramid while the iodine ligands occupy the apical positions with ∠(I1-Bi1-I2) = 177.014(10) °. One should note here that the THF ligand is located at a special position so that two equivalent positions result, each with one shorter contact *d*(Bi···O) = 3.072(7) Å to one and an appreciably longer one of *d*(Bi3.735(7) Å to the other Bi atom. On average, it thus acts as a bridging ligand. Coordination of the pyridinyl nitrogen atoms of the ligand is confirmed by the bond lengths of *d*(Bi1-N1) =2.527(4) Å and *d*(Bi1-N3) = 2.503(4) Å, which are shorter than the sum of the van der Waals radii, while the anionic character of the pyrrolide central ring becomes evident from the shortened bond length of *d*(Bi1-N2) = 2.182(4) Å. In addition to the dimeric coordination, the ligands exhibit π-stacking interactions such that two pyridine rings are stacked on top of one another and one pyridinyl is associated with the pyrrolide central unit of another molecule (depicted in **Figure 1**). These interactions then lead to the appearance of a zig–zag pattern of the solid-state structure, if viewed along the b-axis (refer to Figure S26, Supporting Information). Values for the bond lengths, angles, dihedral angles, and short contacts are provided within Table S1–S5, Supporting Information.

Intriguingly, degradation of **As(DPP)I_2** in dmso is a selective process, leading to one specific complex, besides small quantities of the free proligand **HDPP**, as shown by NMR monitoring (Figure S23, Supporting Information). We were able to isolate this compound from the slow hydrolysis of **As(DPP)I_2** in undried dmso and succeeded in recording NMR spectra and growing single crystals that lent themselves to X-ray diffraction. These studies revealed the decomposition product to be a dicationic oxo-bridged dimer with two triiodide anions, i. e., **[{As(DPP)}$_2$(μ-O)]$^{2+}$ 2 I_3^-** (refer to **Figure 2** and Figure S27 and S28, Supporting Information). The two DPP^- ligands of the cationic dimer are nearly coplanar within this solid-state structure, with a tilt angle between the two pyrrolide rings of 7.6(5)° and centroid to plane normal distance of 3.39(1) Å. The ligands are twisted slightly against each other with θ(N5-As2-As1-N2) = 12.2(4) °, where N5 and N2 are the pyrrolide N atoms. The nitrogen–arsenic bond lengths are considerably smaller for the anionic pyrrolide nitrogen atoms with *d*(As1-N2) = 1.877(11) Å and *d*(As2-N5) = 1.874(11) Å than for the neutral pyridine donor nitrogen atoms with *d*(As1-N3) = 2.196(10) Å, *d*(As1-N1) = 2.287(10) Å, *d*(As2-N4) = 2.249(10) Å, and *d*(As-N6) =2.228(9) Å. The bridging oxygen atom forms an angle of ∠(As1-O1-As2) = 147.5(6)°. The intermolecular interactions within this solid-state structure are

Table 1. ^{1}H NMR shifts of the complexes **Pn(DPP)I_2** in dmso-d_6.

	HDPP	Bi(DPP)I_2	Sb(DPP)I_2	As(DPP)I_2
H-1	6.92	6.97	7.19	7.33
H-4	7.88	7.95	8.10	8.18
H-5	7.78	8.02	8.18	8.27
H-6	7.19	7.35	7.49	7.57
H-7	8.55	9.00	9.07	9.00

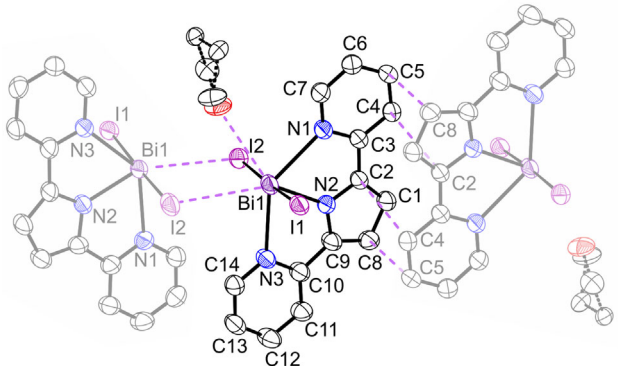

Figure 1. Structure of dimerically-associated molecules of **Bi(DPP)I_2** within the solid-state structure obtained from single-crystal X-ray diffraction. The asymmetric unit is depicted in a bolder color while the molecules not contained within the asymmetric unit are shown in a paler color. The THF solvent molecule resides at a special position, only one of which is shown. Refer to Figure S26, Supporting Information, for a view of both orientations. The Oak ridge thermal ellipsoid plot (ORTEP) is set to the 50% probability level, and H atoms are omitted for clarity.

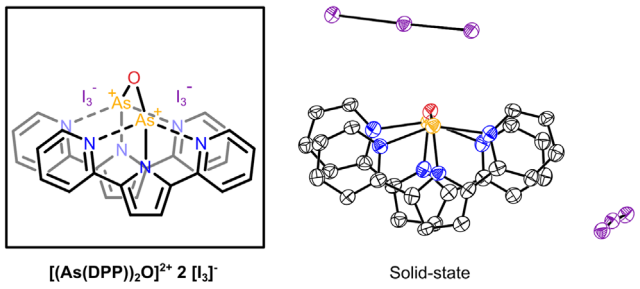

Figure 2. Left: Structure of $[\{As(DPP)\}_2(\mu\text{-}O)]^{2+}$ **2** I_3^-, the decomposition product of **As(DPP)I$_2$** formed upon exposure to dmso containing trace moisture. Right: Solid-state structure of $[\{As(DPP)\}_2(\mu\text{-}O)]^{2+}$ **2** I_3^- as obtained from single-crystal X-ray diffraction with ORTEPs set to the 30% probability level and H atoms omitted for clarity reasons.

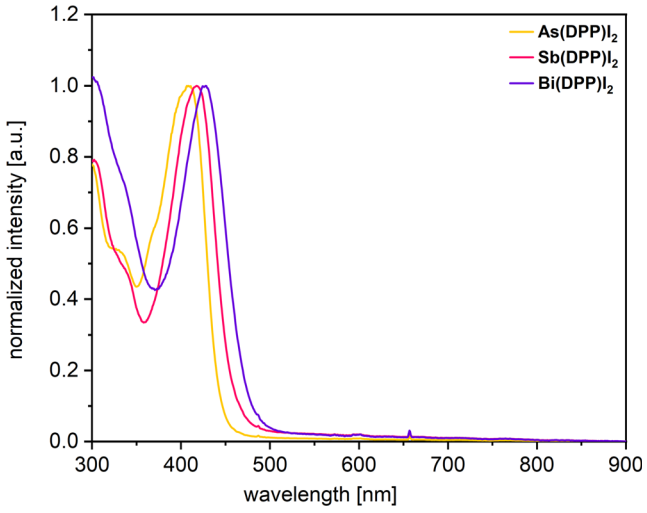

Figure 3. Comparison of the UV–vis absorption spectra of dmso solutions of the three complexes **Pn(DPP)I$_2$**. The spectra are normalized to the HOMO–LUMO transition for clarity and ease of comparison. The complexes appear yellow in color (cf. Figure S30, Supporting Information for a photograph) as a result of the prominent band at $\lambda_{max} > 400$ nm in the vis region of the spectrum.

dominated by iodine–iodine and hydrogen–iodine interactions between I_3^- iodine atoms and hydrogen atoms at the DPP^- ligands (refer to Table S10, Supporting Information for the values) and one As···C contact of d(As1···C10) = 3.588(12) Å. These contacts lead to the formation of channels of $[\{As(DPP)\}_2(\mu\text{-}O)]^{2+}$ ions within the solid-state structure that are separated by ribbons of I_3^- anions (cf. Figure S28, Supporting Information for a depiction).

In addition to its solid state structure, we characterized this compound via NMR spectroscopy in dmso-d_6 (see Figure S17–S21, Supporting Information) and confirmed that the ^{1}H-NMR shifts are indeed identical to the product which forms from **As(DPP)I$_2$** in dmso-d_6 (refer to Figure S23, Supporting Information). As the conversion of **As(DPP)I$_2$** to $[\{As(DPP)\}_2(\mu\text{-}O)]^{2+}$ seems to be tied to the water content of dmso, we assume nucleophilic substitution of iodide ligands with formation of two equivalents of HI, which then, according to the Bodenstein equilibrium, form I_2 and H_2, the former being trapped upon loss of the remaining iodide ligands from the As atoms as triiodide ions.

2.1. UV–Vis Absorption and Time-Dependent Density Functional Theory (TD-DFT) Calculations

UV–vis absorption spectra of the three complexes **Pn(DPP)I$_2$** in dsmo are provided in **Figure 3**; values for absorption maxima and absorption coefficients are compiled in **Table 2**. For clarity and ease of comparison, the absorption spectra are normalized to the lowest energy transition within Figure 3.

The absorption spectra are nearly identical, yet a slight but systematic redshift is observed with increasing atomic number such that absorption maxima of the lowest energy transitions lie at 409 nm for **As(DPP)I$_2$**, at 417 nm for **Sb(DPP)I$_2$**, and at 427 nm for **Bi(DPP)I$_2$**. This trend parallels the increasing Lewis acidity of the respective central pnictogen, which may lead to a greater stabilization of the partially metal-centered LUMO while less affecting the energy of the ligand-centered HOMO, thus reducing the HOMO–LUMO energy gap. In addition to the slight bathochromic shift, the absorption coefficients follow the ordering **As(DPP)I$_2$** > **Sb(DPP)I$_2$** > **Bi(DPP)I$_2$**, correlating with the increasing molecular weights across this series.

Table 2. Comparison of the UV–vis absorptive properties of **Pn(DPP)I$_2$** recorded in solutions of dmso for **Sb(DPP)I$_2$** and **Bi(DPP)I$_2$** or CH_2Cl_2 for **As(DPP)I$_2$** at r.t.

	λ_{max} [nm] (ε_λ [× 10^3 M^{-1} cm^{-1}])
As(DPP)I$_2$[a]	343 (4.0),[c] 418 (10.7)
Sb(DPP)I$_2$[b]	300 (8.1), 336 (5.0),[c] 417 (10.2)
Bi(DPP)I$_2$[b]	300 (9.8), 333 (7.1),[c] 427 (9.6)

[a]in CH_2Cl_2; [b]in dmso; [c]shoulder absorption.

In order to aid in the interpretation of the UV–vis absorption spectra, we performed quantum chemical calculations at the TD-DFT level of theory on the complexes **Pn(DPP)I$_2$**. These calculations provide good agreement between computed and experimental spectra in terms of oscillator strengths and energies. Figure S37–S39, Supporting Information, provide the comparison between calculated and experimental spectra. The full overview of all relevant electronic transitions and the involved MOs is provided exemplarily for **Bi(DPP)I$_2$** in **Figure 4**; equivalent depictions for the lighter congeners are given as Figure S37–39, Supporting Information. From the rendered depictions of the MOs of **Bi(DPP)I$_2$** (white and blue in Figure 4), it becomes evident that the HOMO–LUMO transition has partial charge transfer (CT) character, in which electron density is shifted from mainly the electron-rich central pyrrolide unit of the DPP^- ligand to an acceptor orbital which represents bismuth-halide σ-antibonding and Bi-N π-bonding interactions. The latter are mingled with intraligand π–π^* transitions within the DPP^- chromophore as evidenced by the electron density difference maps (EDDMs), where electron density loss during the transition is marked in blue and electron density gain in red color. Higher-energy bands at 333–343 and 300 nm correspond to CT excitations, in which electron density

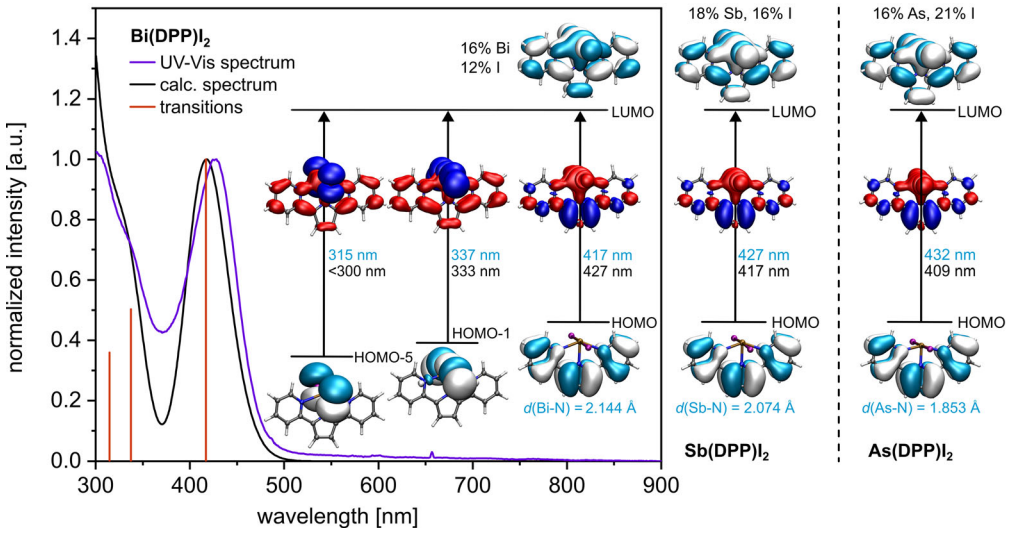

Figure 4. Left: Comparison of the experimental and calculated UV–vis absorption spectra of **Bi(DPP)I$_2$** in dmso along with the relevant calculated electronic transitions as red bars and the calculated wavelengths. The respective acceptor and donor MOs are shown in light blue and white colors, and the corresponding EDDMs in red and blue, with electron density gain in red and electron density loss in blue. The numbers in black represent the wavelengths of the experimentally detected electronic transitions, while light blue numbers denote the TD-DFT calculated wavelengths. Right: MOs and EDDMs involved in the HOMO–LUMO transition of **Sb(DPP)I$_2$** and **As(DPP)I$_2$**. Percentages provided at the LUMO correspond to the contributions as obtained from TD-DFT calculations. d(Pn—$N_{pyrrolide}$) bond lengths as obtained from TD-DFT calculations are provided in blue color.

is shifted from the free electron pairs at the iodide ligands and the pnictogen–iodide bonding orbitals to the DPP$^-$ ligand. The large similarity between the three representatives **Pn(DPP)I$_2$** with Pn = Bi, Sb, As becomes evident from the HOMO–LUMO transition, which is depicted on the right side of Figure 4. Indeed, the character of every transition remains the same across the series, although the energies are shifted slightly. A minor difference is the contribution of the respective pnictogen ion Pn^{3+} to, in particular, the LUMO, which was computed to lie at 16% for Bi^{3+} and As^{3+}, while the value for Sb^{3+} is slightly larger at 18%. Additionally, the contributions of the iodide ligands to the LUMO decrease along the series, from 21% for the LUMO of **As(DPP)I$_2$**, to 16% in **Sb(DPP)I$_2$**, and to 12% in **Bi(DPP)I$_2$**. Contributions of every molecular component are compiled for each of the complexes within Table S11–S13, Supporting Information, and values for the LUMO are indicated in Figure 4.

2.2. Photoluminescence Studies

Figure 5 provides the photoluminescence emission and excitation spectra, while pertinent data are compiled in **Table 3**. Additional data, including the monoexponential fitting of the decay traces, are provided within Figure S31–S34, Supporting Information.

Upon irradiation of glasses formed from dilute solutions of the complexes **Pn(DPP)I$_2$** in 2-methyltetrahydrofuran (2-MeTHF) at cryogenic temperatures, we observe bright orange to red emission (see Figure S36, Supporting Information for a photograph). The latter is assigned as phosphorescence owing to the large energy difference of $\Delta E_{em\ exc/phos} > 5000\ cm^{-1}$

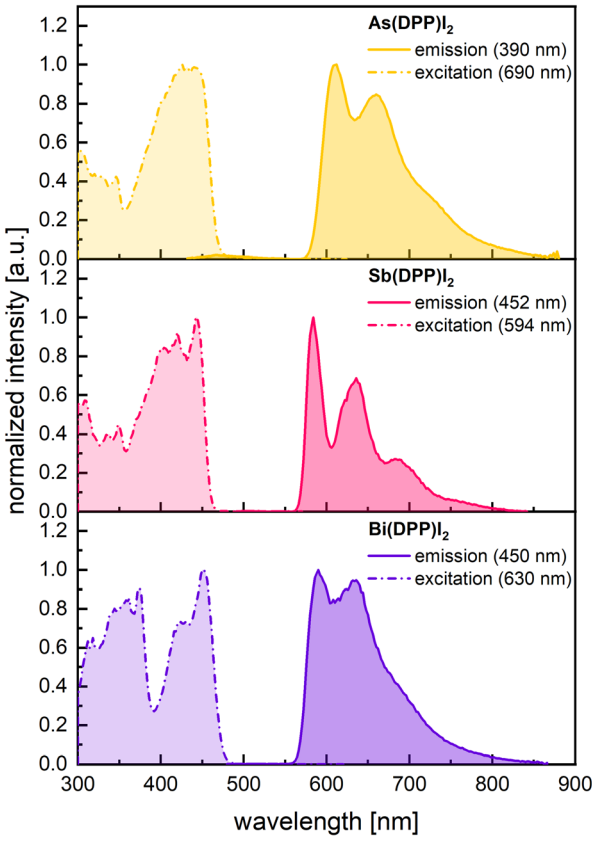

Figure 5. Emission (solid line, darker shaded area) and excitation spectra (dashed line, lighter shaded area) for the emission of the complexes **Pn(DPP)I$_2$** in 2-MeTHF at 77 K.

Table 3. Comparison of the emissive properties of complexes **Pn(DPP)I$_2$** recorded in solutions of CH_2Cl_2 at r.t. or in 2-MeTHF at 77 K.

	As(DPP)I$_2$	**Sb(DPP)I$_2$**	**Bi(DPP)I$_2$**
$\lambda_{em,flu}$ [nm]	470[a]/466[b]	n.a.	n.a.
$\Delta E_{em\text{-}exc,flu}$ [cm^{-1}]	2647[a]/1270[b]	n.a.	n.a.
τ_{flu} [ns]	2.4(1%), 0.48 (99%)[a]	n.a.	n.a.
Φ_{flu} [%]	2.1[a]	n.a.	n.a.
$\lambda_{em,phos}$ [nm][b]	612	584	589
$\Delta E_{em\text{-}exc,phos}$ [cm^{-1}][b]	6650	5450	5244
τ_{phos} [µs][b]	60	219	128
Φ_{phos} [%][b]	62.8	83.9	50.8
Φ_{Δ} [%][c]	14	9	<1

[a]in CH_2Cl_2 at r.t.; [b]in 2-MeTHF at 77 K; [c]in $CHCl_3$ at r.t. vs. TPP.

between the energetically lowest excitation and the emission maxima. The emission shifts to higher energy in the order **As(DPP)I$_2$** < **Sb(DPP)I$_2$** ≈ **Bi(DPP)I$_2$** (refer to Table 3). Further supportive of the assignment as phosphorescence are the long lifetimes extracted from time-resolved emission decay curves (cf. Figure S31, S33, S34, Supporting Information), which range from τ_{phos} = 219 µs for **Sb(DPP)I$_2$**, over τ_{phos} = 128 µs for **Bi(DPP)I$_2$**, to τ_{phos} = 60 µs for **As(DPP)I$_2$**. In further support of phosphorescence emission, the emission from the triplet state was calculated to lie at $\lambda_{phos,calc}$ = 670 nm for **As(DPP)I$_2$**, at $\lambda_{phos,calc}$ = 618 nm for **Sb(DPP)I$_2$**, and at $\lambda_{phos,calc}$ = 600 nm for **Bi(DPP)I$_2$**, which is in good to excellent agreement with the experimental values.

Contrary to expectations, the As complex exhibits the shortest luminescence lifetime. A possible rationale for this observation is that computed iodide contributions to the LUMO of **As(DPP)I$_2$** are considerably larger than for **Sb(DPP)I$_2$** and **Bi(DPP)I$_2$**, while the smaller ionic radius of As^{3+} leads to smaller nitrogen pnictogen bond lengths and a more covalent character of the Pn-ligand bonds, and therefore, better orbital overlap between the metal-centered excited state and the ligand-centered ground state. This is reflected in the TD-DFT calculations in which the Pn—N bond lengths within the optimized structures are *d*(As-N2) = 1.853 Å, while those of the heavier congeners are considerably elongated with *d*(Sb-N2) = 2.074 Å and *d*(Bi-N2) = 2.144 Å. These values compare favorably to Pn—$N_{pyrrolide}$ bond lengths in literature[19] and to the experimental value of *d*(Bi1-N2) = 2.182(4) Å obtained for **Bi(DPP)I$_2$** from X-ray diffraction. Thus, we assume that the phosphorescence lifetimes of these complexes are governed by several effects: i) the orbital overlap between the Pn^{3+} central atom and the N-donors, which increases as the bonds become shorter, ii) the SOC constant of the Pn^{3+} ion, and iii) iodide contributions to the LUMO. The short lifetime of **Bi(DPP)I$_2$** in comparison with **Sb(DPP)I$_2$** is likely governed by the larger SOC constant of bismuth and the resulting ability of Bi to overcome the spin-forbidden character of the T_1-S_0 transition.

Quantum yields for the phosphorescence emission at 77 K are high with values ranging from Φ_{phos} = 50.8% for **Bi(DPP)I$_2$**, Φ_{phos} = 62.8% for **As(DPP)I$_2$**, and arriving at Φ_{phos} = 83.9% for **Sb(DPP)I$_2$**. This attests not only to the propensity of bismuth, but also of the lighter representatives Sb^{3+} and As^{3+} to induce efficient ISC. As for previous studies, we assume that the partial CT character of the HOMO–LUMO transition with the involvement of the pnictogen ion in the electronic transition is important for attaining efficient ISC. In the present complexes, the HAE of the iodide ligand is also deemed to play a role.

A closer look at the emission of **As(DPP)I$_2$** in 2-MeTHF at cryogenic temperatures reveals a second emissive feature with low intensity between 400 and 550 nm and a maximum at λ_{em} = 466 nm. This feature possesses a lifetime in the nanosecond range, but it is too weak in intensity to measure the lifetime accurately. We assign this emission to additional fluorescent emission of the arsenic complex that the heavier congeners lack, owing to their larger SOC constants and resulting higher ISC efficiencies. In accordance with this assignment, we found **As(DPP)I$_2$** to be weakly fluorescent in dichloromethane solution at r.t. (refer to **Figure 6**) with a maximum $\lambda_{em,flu}$ = 470 nm, and a biexponential lifetime of $\tau_{flu,1}$ = 0.5 ns (99%) and $\tau_{flu,2}$ = 2.4 ns (1%). Under these conditions, the quantum yield for this emission lies at Φ_{flu} = 2.1%. The rather large Stokes shift of 2647 cm^{-1} is suggestive of large structural differences between the ground and excited states. We were unable to detect similar emissive features for either of the heavier congeners in either CH_2Cl_2 or dmso solution at r.t.

With view on the rather efficient ISC of all three compounds as revealed by the large phosphorescence quantum yields at cryogenic temperature and the lack or the weak intensity of fluorescence emission in CH_2Cl_2 solution at r.t., we measured the singlet oxygen ($^1O_2$) quantum yields Φ_{Δ} of the three complexes **Pn(DPP)I$_2$** at r.t. in $CHCl_3$ relatively to 5,10,15,20-tetraphenyl-21*H*,23*H*-porphin (TPP) through the intensity of the $^1O_2$ phosphorescence emission. Corresponding spectra are supplied in **Figure 7**.

We observe a systematic increase of Φ_{Δ} across this series with values ranging from Φ_{Δ} < 1% for **Bi(DPP)I$_2$**, to Φ_{Δ} = 9% for **Sb(DPP)I$_2$**, and arriving at Φ_{Δ} = 14% for **As(DPP)I$_2$**. As evidenced by the presence of $^1O_2$, the excited triplet state is indeed occupied at r.t., but decays nonradiatively under these conditions. We assume this occurs via a fast ISC process, in which the molecule accesses excited vibronic levels of the singlet ground state and decays from there via vibrational relaxation. This assumption aligns both with the increasing SOC constants along this series, as well as with the decreasing capability for $^1O_2$ generation.

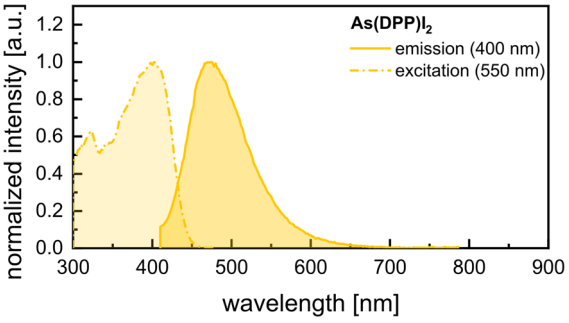

Figure 6. Emission (solid line, darker shaded area) and excitation spectra (dashed line, lighter shaded area) for the emission **As(DPP)I$_2$** in CH_2Cl_2 at r.t.

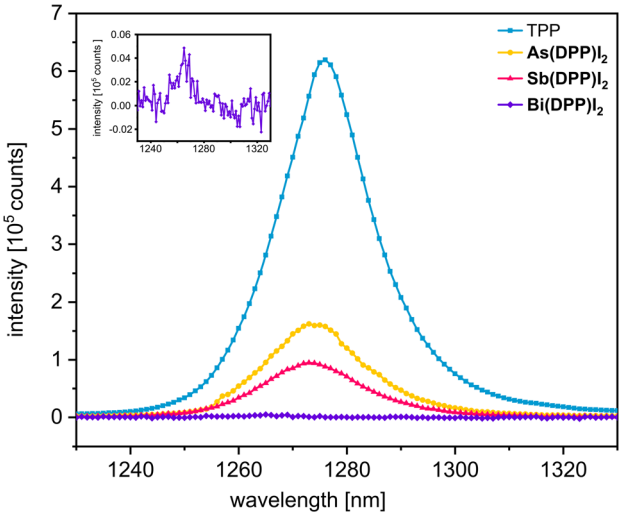

Figure 7. $^1O_2$ quantum yield measurements of **Pn(DPP)I$_2$** in comparison to 5,10,15,20-tetraphenyl-21*H*,23*H*-porphin (TPP). Spectra were recorded from solutions in $CHCl_3$ at r.t. under excitation at $\lambda_{exc} = 421$ nm.

3. Conclusions

Three new pnictogen complexes **Pn(DPP)I$_2$** bearing the 2,2′-(pyrrole-1-ide-2,5-diyl)bis(pyridine) ligand DPP^- were successfully synthesized and characterized. **As(DPP)I$_2$** is sensitive toward hydrolysis, delivering the oxo-bridged dicationic complex $[\{As(DPP)\}_2(\mu\text{-}O)]^{2+}$, which was isolated and structurally characterized as the triiodide salt. The three **Pn(DPP)I$_2$** complexes display systematic shifts in their ^{1}H-NMR and UV–vis absorption spectra in accordance with the decreasing electronegativity of the pnictogen atom. Experimental and TD-DFT calculated electronic absorption spectra reveal a profound similarity between the three complexes with partial CT character for each transition. In particular, the HOMO–LUMO transition possesses partial DPP^- to Pn^{3+} ligand-to-metal charge-transfer character with electron density shifting from the electron-rich pyrrolide unit to the pnictogen-iodide antibonding and Pn-N π-bonding LUMO. We found all three complexes to be phosphorescent in glassy matrices of 2-MeTHF at 77 K in the orange to red range of the spectrum with high quantum yields, maximizing at $\Phi_{phos} = 83.9\%$ for **Sb(DPP)I$_2$**. Phosphorescence lifetimes τ_{phos} lie in the range of 60–219 microseconds, with the highest value for **Sb(DPP)I$_2$**. Surprisingly, the lifetime of the phosphorescent emission of **As(DPP)I$_2$** is the shortest within this series. We conclude that the phosphorescence lifetimes of pnictogen complexes do not solely relate to the SOC constant of the Pn^{3+} atom. Instead, the orbital overlap as regulated through Pn—N bond lengths and the contributions of the Pn atom and, in particular, the iodide ligands to the involved MOs must be considered as well. We found **As(DPP)I$_2$** to be weakly fluorescent at both 77 K and at r.t. in CH_2Cl_2 solution, while the heavier complexes **Sb(DPP)I$_2$** and **Bi(DPP)I$_2$** are nonemissive at r.t. This is attributed to the large ISC efficiencies of both Sb^{3+} and Bi^{3+} through their large SOC constants. Nevertheless, this study highlights the capability of all three elements for generating phosphorescent materials and as sensitizers for $^1O_2$ generation.

4. Experimental Section

Synthetic Procedures: Syntheses of all compounds were carried out according to modified literature procedures as detailed below, using standard Schlenk techniques or a nitrogen-filled glovebox when specified. Solvents (benzene, THF, CH_2Cl_2, and dmso) were dried over a MBRAUN solvent purification system, kept over molecular sieves (4 Å), and stored under a nitrogen atmosphere prior to use. Water contents were determined to be <2 ppm using a Karl-Fischer-Coulometer from SI Analytics in regular time intervals. Other solvents (CD_2Cl_2, 2-MeTHF, dmso-d_6) were dried and stored over molecular sieves (4 Å). Commercially available starting materials were used as received.

^{1}H- and ^{13}C-NMR Spectroscopy: ^{1}H-NMR spectra were measured on a Bruker Avance III 400 spectrometer ($B_H = 400$ MHz) at r.t. in $CDCl_3$, CD_2Cl_2, or dmso-d_6. ^{13}C-NMR spectra were recorded on a Bruker Avance III 400 spectrometer ($B_C = 101$ MHz) in dmso-d_6 and CD_2Cl_2. All spectra were referenced against the residual protonated solvent (^{1}H, $\delta = 7.26$ ppm for $CHDCl_2$, and 2.50 ppm for dmso). NMR spectra of **As(DPP)I$_2$** and **Sb(DPP)I$_2$** were recorded in custom-built 5 mm boroeco 5–7 NMR tubes fitted with a J. YOUNG`s Teflon cap and an insert.

Mass Spectrometry: Mass spectra were recorded using an Agilent 6546 LC/Q-TOF spectrometer in the positive ion mode (flow rate: 0.5 mL min^{-1}, source temperature: 320 °C, and capillary voltages: 3500 V) with the direct injection of the CH_2Cl_2 solutions.

UV–Vis Absorption Spectroscopy: UV–vis absorption spectra were recorded on a TIDAS fiber optic diode array spectrometer, consisting of a combination of MCS UV/Vis and PGS NIR instruments from j&m Analytic AG. Extinction coefficients were measured using quartz cells from Hellma Analytics with optical path lengths of 1 cm, or in a custom-built quartz cuvette with a vacuum valve, whereby the original cuvette was a 1 cm cell with a 221.01Qs tube purchased from Hellma Analytics.

X-Ray Diffraction Analysis: Single-crystal X-ray Diffraction (SC-XRD) was conducted on a STOE IPDS II diffractometer from STOE & Cie GmbH equipped with a graphite monochromator and a Cu Kα-radiation source ($K_\alpha = 1.54186$ Å) at 100 K. The X-Area program package was used for data processing, and absorption correction was conducted both semiempirically and spherically. The structure was solved with SHELXT[20] and the OLEX2[21] program packages. All nonhydrogen atoms were refined anisotropically. Intermolecular interactions were analyzed using the Mercury and OLEX2 program packages. Deposition numbers 2449324 and 2454109 contain the supplementary crystallographic data for this paper.

Quantum Chemistry: Quantum chemical calculations based on density functional theory (DFT) employed the Gaussian 16 program package.[22] Geometry optimization was followed by vibrational analysis. All calculations were performed applying the polarizable continuum model (SMD) in dmso.[23] Electronic spectra were calculated at the optimized ground-state structures by the TD-DFT method. In conjunction with the Perdew, Burke Ernzerhof exchange and correlation functional PBE0,[24] the fully realistic small-core multiconfiguration Dirac-Hartree-Fock-adjusted pseudopotential and the corresponding set for Bi (ECP60MDF),[25] the RI-MP2 optimized auxiliary basis sets for As,[26] and the def2-QZVPP basis set for Sb,[27] LAN2DZ[28] for iodine, and 6-31(G)[29] polarizable double-ζ basis sets for the remaining atoms were used. The GaussSum,[30] Avogadro,[31] GNU Parallel,[32] and vmd[33] program packages were used in combination with POV-Ray[34] for data processing and graphical representations.

Photoluminescence Spectroscopy: Excitation and emission spectra and the respective lifetimes of the excited states were recorded with the FluoTime 300 spectrometer from PicoQuant. All measurements were performed in dry 2-MeTHF or CH_2Cl_2 on solutions with an absorbance <0.1. Spectra at 77 K in 2-MeTHF were recorded in quartz tubes. Spectra recorded at r.t. were subjected to four freeze-pump-thaw cycles prior to measurement to ensure that no quenching through residual O_2 could take place. UV–vis absorption spectra were recorded prior to and after measurements and compared to guarantee no degradation during the measurement. Absolute quantum yields were determined using an integrating sphere within the FluoTime 300 spectrometer. Quantum yields at 77 K were measured in 2-MeTHF in quartz tubes with an absolute quantum yield setup for low temperatures using the A11238−02 Dewar and a C9920 02G spectrometer purchased from Hamamatsu. Singlet oxygen quantum yields were measured relatively to 5,10,15,20-tetraphenyl-21*H*,23*H*-porphin (TPP), which possesses a singlet oxygen quantum yield of $\Phi_\Delta = 0.55$ in $CHCl_3$ solution under air[35] using a previously reported method.[36]

Synthesis and Characterization: 2,2′-(1H-Pyrrole-2,5-diyl)bis[pyridine]:

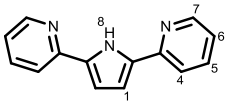

Sodium acetate (322 mg, 3.92 mmol, 0.10 eq) and 3-benzyl-5-(2-hydroxyethyl)-4-methylthiazol-3-ium chloride (1.06 g, 3.92 mmol, 0.10 eq.) were dissolved in EtOH (120 mL, dry, degassed) in a 250 mL Schlenk flask and heated to reflux. 2-Pyridinecarboxaldehyde (3.7 mL, 39.21 mmol, 1.00 eq.) was added, turning the previously pale-yellow solution dark blue. Divinyl sulfone (1.0 mL, 9.80 mmol, 0.25 eq.) was added, resulting in a bright orange solution. The reaction mixture was heated to reflux for 14 h, after which time a bright yellow precipitate had formed. The reaction was cooled to r.t., and the precipitate was collected via Büchner filtration. This precipitate was added to neat ammonium acetate (75 g) and the mixture was heated at 140 °C for 2 h. The mixture was poured into distilled water (100 mL), and the resulting dark brown aqueous phase was extracted with CH_2Cl_2 (techn. grade, 6 × 100 mL) until the organic phase was colorless. The combined organic phases were dried over $MgSO_4$, and the solvent was removed in vacuo to yield a dark oil, which was extracted with boiling *n*-heptane (techn., 3 × 100 mL). The solvent was removed in vacuo to afford colorless crystals of 2,2′-(1*H*-pyrrole-2,5-diyl)bis[pyridine] (1.21 g, 5.45 mmol, 28%).

^{1}H-NMR (400 MHz, 298 K, $CDCl_3$) δ [ppm] = 10.60 (s, 2H, H8), 8.52 (m, 2H, H7), 7.62 (vtd, $^3J_{HH}$ = 7.9 Hz, $^4J_{HH}$ = 1.7 Hz, 2H, H5), 7.56 (vdt, $^3J_{HH}$ = 8.0 Hz, $^4J_{HH}$ = 1.1 Hz, 2H, H4), 7.05 (ddd, $^3J_{HH}$ = 7.9 Hz, $^3J_{HH}$ = 5.0 Hz, $^4J_{HH}$ = 1.1 Hz, H6), 6.77 (d, $^4J_{HH}$ = 2.8 Hz, 2H, H1).

As(DPP)I_2:

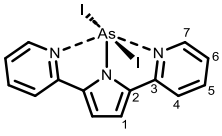

In a nitrogen-filled glovebox, 2,2′-(1*H*-pyrrole-2,5-diyl)bis(pyridine) (150 mg, 677.9 µmol, 1.00 eq.) was dissolved in THF (4 mL, dry) and added to KH (30 mg, 745.7 µmol, 1.10 eq.). The reaction mixture was stirred for 36 h until the production of hydrogen ceased, affording a dark solution with a colorless, cloudy precipitate. The suspension was added to a solution of AsI_3 (308.9 mg, 677.9 µmol, 1.00 eq.) in THF (1 mL, dry), resulting in the immediate precipitation of an orange solid. After 2 h, stirring was stopped and the precipitate was allowed to settle. The precipitate was collected and washed with THF (3 × 2 mL, dry). The residue was extracted with dry CH_2Cl_2 (2 × 10 mL) using a predried polytetrafluoroethylene (PTFE) syringe filter. The solvent was removed in vacuo to give **As(DPP)I_2** as a red–orange solid in quantitative yield (372.17 mg, 677.9 µmol, 1.00 eq.).

^{1}H-NMR (400 MHz, 298 K, CD_2Cl_2) δ [ppm] = 8.74 (ddd, $^3J_{HH}$ = 5.5 Hz, $^4J_{HH}$ = 1.0 Hz, $^5J_{HH}$ = 0.4 Hz, 2H, H7), 8.10 (ddd, $^3J_{HH}$ = 8.1 Hz, $^3J_{HH}$ = 7.4 Hz, $^4J_{HH}$ = 1.0 Hz, 2H, H5), 7.86 (dvt, $^3J_{HH}$ = 8.1 Hz, $^4J_{HH}$ = 1.2 Hz, 2H, H4), 7.43 (ddd, $^3J_{HH}$ = 7.4 Hz, $^3J_{HH}$ = 5.5 Hz, $^4J_{HH}$ = 1.2 Hz, 2H, H6), 7.18 (s, 2H, H1).

^{13}C-NMR (101 MHz, 298 K, CD_2Cl_2) δ [ppm] = 147.4 (C3), 144.4 (C7), 141.7 (C5), 135.4 (C2), 123.2 (C6), 120.4 (C4), 114.8 (C1).

ESI-MS $C_{14}H_{10}N_3AsI^+$ calculated 421.9130, found 421.9130.

Sb(DPP)I_2:

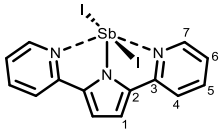

In a nitrogen-filled glovebox, 2,2′-(1*H*-pyrrole-2,5-diyl)bis(pyridine) (150 mg, 677.9 µmol, 1.00 eq.) was dissolved in THF (4 mL, dry) and added to KH (30 mg, 745.7 µmol, 1.10 eq.). The reaction mixture was stirred for 36 h until the production of hydrogen ceased, affording a dark solution with a colorless, cloudy precipitate. The suspension was added to a solution of SbI_3 (340.7 mg, 677.9 µmol, 1.00 eq.) in THF (1 mL, dry), resulting in the immediate precipitation of an ocher solid. After 2 h, stirring was stopped and the precipitate was allowed to settle. The precipitate was collected and washed with THF (3 × 2 mL, dry). The residue was extracted with dry CH_2Cl_2 (4 x 10 mL) using a predried PTFE syringe filter. The solvent was removed in vacuo to give **Sb(DPP)I_2** as a yellow solid in 95% yield (384.02 mg, 677 µmol, 0.95 eq.).

^{1}H-NMR (400 MHz, 298 K, $(CD_3)_2SO$) δ [ppm] = 9.07 (d, $^3J_{HH}$ = 5.4 Hz, 2H, H7), 8.18 (ddd, $^3J_{HH}$ = 8.0 Hz, $^3J_{HH}$ = 7.3 Hz, $^4J_{HH}$ = 1.5 Hz, 2H, H5), 8.10 (dvt, $^3J_{HH}$ = 8.0 Hz, $^4J_{HH}$ = 1.0 Hz, 2H, H4), 7.49 (ddd, $^3J_{HH}$ = 7.3 Hz, $^3J_{HH}$ = 5.4 Hz, $^4J_{HH}$ = 1.3 Hz, 2H, H6), 7.19 (s, 2H, H1).

^{13}C-NMR (101 MHz, 298 K, $(CD_3)_2SO$) δ [ppm] = 148.8 (C3), 146.7 (C7), 141.6 (C5), 136.5 (C2), 122.2 (C6), 119.8 (C4), 114.1 (C1).

ESI-MS $C_{14}H_{10}N_3SbI^+$ calculated 467.8952, found 467.8957.

Bi(DPP)I_2:

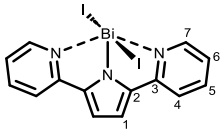

In a nitrogen-filled glovebox, 2,2′-(1*H*-pyrrole-2,5-diyl)bis(pyridine) (150 mg, 677.9 µmol, 1.0 eq.)was dissolved in THF (4 mL, dry) and added to KH (30 mg, 745.7 µmol, 1.1 eq.). The reaction mixture was stirred for 36 h until the production of hydrogen stopped, affording a dark solution with a colorless, cloudy precipitate. The suspension was added to a solution of BiI_3 (399.8 mg, 677.9 µmol, 1.0 eq.) in THF (1 mL, dry), resulting in the immediate precipitation of an orange solid. After 2 h, stirring was stopped and the precipitate was allowed to settle. The precipitate was collected and washed with THF (3 × 2 mL, dry). The remaining workup was conducted under ambient conditions. Extraction of the remaining solid with hot THF (3 × 25 mL, dry) afforded a bright orange solution. Removal of the solvent afforded **Bi(DPP)I_2** as a bright orange solid (38 mg, 56 µmol, 8%). An additional crop of **Bi(DPP)I_2** was obtained from the THF supernatant of the reaction mixture, which gave an orange precipitate of **Bi(DPP)I_2** within three days (181 mg, 264 µmol, 39%), such that **Bi(DPP)I_2** was obtained in a total yield of 47%. Single crystals suitable for SC-XRD were obtained by slow evaporation of saturated solutions of **Bi(DPP)I_2** in THF.

^{1}H-NMR (400 MHz, 298 K, $(CD_3)_2SO$) δ [ppm] = 9.00 (d, $^3J_{HH}$ = 5.5 Hz, 2H, H7), 8.03 (ddd, $^3J_{HH}$ = 8.1 Hz, $^3J_{HH}$ = 7.2 Hz, $^4J_{HH}$ = 1.6 Hz, 2H, H5), 7.95 (dvt, $^3J_{HH}$ = 8.1 Hz, $^4J_{HH}$ = 1.3 Hz, 2H, H4), 7.35 (ddd, $^3J_{HH}$ = 7.2 Hz, $^3J_{HH}$ = 5.5 Hz, $^4J_{HH}$ = 1.3 Hz, 2H, H6), 6.97 (s, 2H, H1).

^{13}C-NMR (101 MHz, 298 K, $(CD_3)_2SO$) δ [ppm] = 152.7 (C3), 148.8 (C7), 144.5 (C2), 139.8 (C5), 121.0 (C6), 119.4 (C4), 113.7 (C1).

ESI-MS $C_{14}H_{10}N_3BiI^+$ calculated 555.9718, found 555.9718.

[{As(DPP)}$_2$(μ-O)]$^{2+}$ 2 I_3^-:

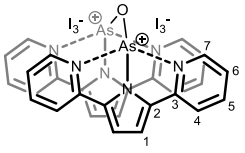

From an NMR sample of **As(DPP)I$_2$** in inadequately dried dmso-d_6, we observed decomposition into a second set of signals differing from both **As(DPP)I$_2$** and the free ligand HDPP. Additionally, a red color of the solution was observed. Crystals suitable for SC-XRD of **[{As(DPP)}$_2$(μ-O)]$^{2+}$ 2 I_3^-** were obtained from slow vapor diffusion of hexane into the aforementioned solution in dmso-d_6. The identity of the as-isolated, crystalline material with the product formed by in situ hydrolysis follows from the identical sets of ^{1}H and ^{13}C NMR resonances.

^{1}H-NMR (400 MHz, 298 K, CD_2Cl_2) δ [ppm] = 8.48 (d, $^3J_{HH}$ = 5.5 Hz, $^4J_{HH}$ = 1.0 Hz, $^5J_{HH}$ = 0.5 Hz, 2H, H7), 8.04 (ddd, $^3J_{HH}$ = 8.0 Hz, $^3J_{HH}$ = 7.5 Hz, $^4J_{HH}$ = 1.5 Hz, 2H, H5), 7.75 (dvt, $^3J_{HH}$ = 8.0 Hz, $^4J_{HH}$ = 1.0 Hz, 2H, H4), 7.29 (ddd, $^3J_{HH}$ = 7.4 Hz, $^3J_{HH}$ = 5.5 Hz, $^4J_{HH}$ = 1.1 Hz, 2H, H6), 6.84 (s, 2H, H1).

^{13}C-NMR (101 MHz, 298 K, CD_2Cl_2) δ [ppm] = 147.3 (C2), 144.0 (C7), 141.8 (C5), 134.6 (C3), 123.4 (C6), 119.6 (C4), 114.1 (C1).

Supporting Information

Supporting Information is available from the Wiley Online Library or from the author.

Acknowledgements

The authors thank Gernot Haug for glovebox maintenance, Michael Linseis for guidance and advice during crystallographic data acquisition and processing, and Malin Bein for mass spectrometry measurements. The authors gratefully acknowledge support by the state of Baden-Württemberg through bwHPC and the German Research Foundation (DFG) through grant no INST 40/575−1 FUGG (JUSTUS 2 cluster), and the NMR Core Facility at the University of Konstanz for experimental support and spectrometer maintenance. K.L.D. would like to thank Katharina Vollmar for humorous discussions during the preparation of the manuscript and Lea Bauer for advice during $^1O_2$ quantum yield measurements.

Open Access funding enabled and organized by Projekt DEAL.

Conflict of Interest

The authors declare no conflict of interest.

Data Availability Statement

The data that support the findings of this study are available in the supplementary material of this article.

Keywords: coordination compounds · heavy atom effect · phosphorescence · photoluminescence · time-dependent density functional theory calculations

[1] a) S. Arunkumar, D. Ghosh, G. R. Kumar, *Results Chem.* **2022**, *4*, 100399; b) S. M. Parke, E. Rivard, *Isr. J. Chem.* **2018**, *58*, 915; c) S. Ito, M. Gon, K. Tanaka, *Eur. J. Inorg. Chem.* **2024**, *27*, e202400180.

[2] a) B. Valeur, M. N. Berberan-Santos, *Molecular Fluorescence*, 2nd ed., Wiley-VCH, Weinheim **2013**; b) M. Montalti, A. Credi, L. Prodi, M. T. Gandolfi, *Handbook of Photochemistry*, 3, CRC Press, Boca Raton **2006**.

[3] a) J. Doležel, A. Poryvai, T. Slanina, J. Filgas, P. Slavíček, *Chem. Eur. J.* **2024**, *30*, e202303154; b) A. Malinge, S. Kumar, D. Chen, E. Zysman-Colman, S. Kéna-Cohen, *J. Phys. Chem. C* **2024**, *128*, 1122.

[4] a) G. L. Miessler, P. J. Fischer, D. A. Tarr, *Inorg. Chem*, 5th ed., Pearson Boston, Boston **2014**; b) C.-W. Hsu, C.-C. Lin, M.-W. Chung, Y. Chi, G.-H. Lee, P.-T. Chou, C.-H. Chang, P.-Y. Chen, *J. Am. Chem. Soc.* **2011**, *133*, 12085; c) L. Maurer, A. O. Pearce, M. F. Maharaj, D. R. Niamh, L. Brown, C. Amador, K. Niels, H. Damrauer, M. Marshak, P, *Inorg. Chem.* **2021**, *60*, 10137.

[5] a) A. S. Gowda, T. S. Lee, M. C. Rosko, J. L. Petersen, F. N. Castellano, C. Milsmann, *Inorg. Chem.* **2022**, *61*, 7338; b) M. Gon, M. Yaegashi, K. Tanaka, Y. Chujo, *Chem. Eur. J.* **2023**, *29*, e202203423.

[6] a) M. K. Pandey, D. Mondal, B. S. Kote, M. S. Balakrishna, *ChemPlusChem* **2023**, *88*, e202200460; b) S. Arunkumar, G. R. Kumar, *J. Organomet. Chem.* **2023**, *1001*, 122849.

[7] a) A. Sumida, K. Naka, H. Imoto, *Chem. Asian J. 12*, e202401767; b) A. Sumida, T. Onishi, H. Imoto, K. Naka, *Dalton Trans.* **2024**, *53*, 1706; c) T. Fujii, T. Kusukawa, H. Imoto, K. Naka, *Chem. Eur. J.* **2023**, *29*, e202202572; d) G. R. Kumar, M. Yang, B. Zhou, F. P. Gabbaï, *Mendeleev Commun.* **2022**, *32*, 66.

[8] a) A. Korzun, S. Crespi, C. Golz, A. Bismuto, *Chem. Sci.* **2023**, *14*, 6579; b) T. Agou, S. Kuroiwa, R. Moriyama, T. Kuroda, K. Kubo, H. Fukumoto, M. Morita, R. Inoue, T. Nabeshima, *Chem. Commun.* **2025** c) C. S. Rhett, J. E. Meredith, D. P. John, *Inorg. Chim. Acta* **2004**.

[9] a) W. Ma, L. Xu, S. Zhang, G. Li, T. Ma, B. Rao, M. Zhang, G. He, *J. Am. Chem. Soc.* **2021**, *143*, 1590; b) R. Ballardini, G. Varani, M. T. Indelli, F. Scandola, *Inorg. Chem.* **1986**, *25*, 3858; c) K. L. Deuter, F. Kather, M. Linseis, M. Bodensteiner, R. F. Winter, *Chem. Eur. J.* **2024**, *31*, e202403761; d) K. L. Deuter, D. J.-J. Balaba, M. Linseis, R. R. F. Winter, *Chem. Commun.* **2025** e) J. Ohshita, K. Yamaji, Y. Ooyama, Y. Adachi, M. Nakamura, S. Watase, *Organometallics* **2019**, *38*, 1516; f) K. L. Deuter, K. Vollmar, J. Rieser, M. Linseis, R. F. Winter, *Dalton Trans.*, **2025**, *54*, 9921.

[10] a) J. Ohshita, S. Matsui, R. Yamamoto, T. Mizumo, Y. Ooyama, Y. Harima, T. Murafuji, K. Tao, Y. Kuramochi, T. Kaikoh, H. Higashimura, *Organometallics* **2010**, *29*, 3239; b) M. Geppert, M. Müller, M. Linseis, R. F. Winter, *Dalton Trans.* **2025**, *54*, 1779; c) H. Amarne, W. Helal, S. Wang, *Luminescence* **2019**, *34*, 731.

[11] a) A. Strasser, A. Vogler, *Inorg. Chem. Commun.* **2004**, *7*, 528; b) A. Stamoulis, M. Mato, P. C. Bruzzese, M. Leutzsch, A. Cadranel, M. Gil-Sepulcre, F. Neese, J. Cornella, *J. Am. Chem. Soc.* **2025**, *147*, 6037.

[12] a) Y. Kang, D. Song, H. Schmider, S. Wang, *Organometallics* **2002**, *21*, 2413; b) T. Hirayama, A. Mukaimine, K. Nishigaki, H. Tsuboi, S. Hirosawa, K. Okuda, M. Ebihara, H. Nagasawa, *Dalton Trans.* **2017**, *46*, 15991; c) M. Matsumura, Y. Matsuhashi, M. Kawakubo, T. Hyodo, Y. Murata, M. Kawahata, K. Yamaguchi, S. Yasuike, *Molecules* **2021**, 26.
[13] R. Inaba, K. Oka, T. Iwami, Y. Miyake, K. Tajima, H. Imoto, K. Naka, *Inorg. Chem.* **2022**, *61*, 7318.
[14] E. J. Lee, J. S. Hong, T. Kim, Y. Kang, E. M. Han, *Bull. Korean Chem. Soc.* **2005**, *26*, 1946.
[15] Z. Zhang, L.-Z. Fu, P. He, X.-Y. Yi, *Dalton Trans.* **2024**, *53*, 17772.
[16] J. N. McPherson, L. A. Galan, H. Iranmanesh, M. Massi, S. B. Colbran, *Dalton Trans.* **2019**, *48*, 9365.
[17] A. McSkimming, V. Diachenko, R. London, K. Olrich, C. J. Onie, M. M. Bhadbhade, M. P. Bucknall, R. W. Read, S. B. Colbran, *Chem. Eur. J.* **2014**, *20*, 11445.
[18] G. H. Imler, Z. Lu, K. A. Kistler, P. J. Carroll, B. B. Wayland, M. J. Zdilla, *Inorg. Chem.* **2012**, *51*, 10122.
[19] a) J. L. Atwood, A. H. Cowley, W. E. Hunter, S. K. Mehrotra, *Inorg. Chem.* **1982**, *21*, 1354; b) I. Vránová, R. Jambor, A. Růžička, A. Hoffmann, S. Herres-Pawlis, L. Dostál, *Dalton Trans.* **2015**, *44*, 395.
[20] a) D. Kratzert, J. J. Holstein, I. Krossing, *J. Appl. Crystallogr.* **2015**, *48*, 933; b) G. Sheldrick, *Acta Cryst. A* **2015**, *71*, 3.
[21] O. V. Dolomanov, L. J. Bourhis, R. J. Gildea, J. A. K. Howard, H. Puschmann, *J. Appl. Crystallogr.* **2009**, *42*, 339.
[22] M. J. Frisch, G. W. Trucks, H. B. Schlegel, G. E. Scuseria, M. A. Robb, J. R. Cheeseman, G. Scalmani, V. Barone, G. A. Petersson, H. Nakatsuji, X. Li, M. Caricato, A. V. Marenich, J. Bloino, B. G. Janesko, R. Gomperts, B. Mennucci, H. P. Hratchian, J. V. Ortiz, A. F. Izmaylov, J. L. Sonnenberg, F. D. Williams, F. Lipparini, F. Egidi, J. Goings, B. Peng, A. Petrone, T. Henderson, D. Ranasinghe, V. G. Zakrzewski, et al., Gaussion 09, Revision D.01, Gaussian Inc., Wallingford CT **2016**.
[23] A. V. Marenich, C. J. Cramer, D. G. Truhlar, *J. Phys. Chem. B* **2009**, *113*, 6378.
[24] a) J. P. Perdew, K. Burke, M. Ernzerhof, *Phys. Rev. Lett.* **1996**, *77*, 3865; b) C. Adamo, V. Barone, *J. Chem. Phys.* **1999**, *110*, 6158.
[25] B. Metz, H. Stoll, M. Dolg, *J. Chem. Phys.* **2000**, *113*, 2563.
[26] F. Weigend, M. Häser, H. Patzelt, R. Ahlrichs, *Chem. Phys. Lett.* **1998**, *294*, 143.
[27] F. Weigend, R. Ahlrichs, *Phys. Chem. Chem. Phys.* **2005**, *7*, 3297.
[28] W. R. Wadt, P. J. Hay, *J. Chem. Phys.* **1985**, *82*, 284.
[29] P. C. Hariharan, J. A. Pople, *Theor. Chim. Acta* **1973**, *28*, 213.
[30] N. M. O'Boyle, A. L. Tenderholt, K. M. Langner, *J. Comput. Chem.* **2008**, *29*, 839.
[31] M. D. Hanwell, D. E. Curtis, D. C. Lonie, T. Vandermeersch, E. Zurek, G. R. Hutchison, *J. Cheminf.* **2012**, *4*, 17.
[32] O. Tange, *USENIX Mag.* **2011**, *36*, 42.
[33] W. Humphrey, A. Dalke, K. Schulten, *J. Mol. Graph.* **1996**, *14*, 27.
[34] Povray https://www.povray.org/ (Accessed 12.05.2025).
[35] a) R. Schmidt, E. Afshari, *J. Phys. Chem. C* **1990**, *94*, 4377; b) F. Wilkinson, W. P. Helman, A. B. Ross, *J. Phys. Chem. Ref. Data* **1993**, *22*, 113.
[36] P. Irmler, F. S. Gogesch, A. Mang, M. Bodensteiner, C. B. Larsen, O. S. Wenger, R. F. Winter, *Dalton Trans.* **2019**, *48*, 11690.

Manuscript received: May 27, 2025
Revised manuscript received: July 18, 2025
Version of record online: August 28, 2025